On the Impacts of PV Array Sizing on the Inverter Reliability and Lifetime

Sangwongwanich, Ariya; Yang, Yongheng; Sera, Dezso; Blaabjerg, Frede; Zhou, Dao

Published in:
I E E E Transactions on Industry Applications

DOI (link to publication from Publisher):
10.1109/TIA.2018.2825955

Publication date:
2018

Document Version
Accepted author manuscript, peer reviewed version

On the Impacts of PV Array Sizing on the Inverter Reliability and Lifetime

Ariya Sangwongwanich, *Student Member, IEEE,* Yongheng Yang, *Senior Member, IEEE,*
Dezso Sera, *Senior Member, IEEE,* Frede Blaabjerg, *Fellow, IEEE,* and Dao Zhou, *Member, IEEE*

***Abstract*—To enable a more wide scale utilization of PV systems, the cost of PV energy should be comparable to or even lower than other energy sources. Due to the relatively low cost of PV modules, oversizing PV arrays becomes a common approach to reduce the cost of PV energy in practice. By doing so, the total energy yield can be increased under weak solar irradiance conditions. However, oversizing the PV array will increase the loading of PV inverters, which may have undesired influence on the PV inverter reliability and lifetime. In that case, it may result in a negative impact on the overall PV energy cost, due to the increased maintenance for the PV inverters. With the above concern, this paper evaluates the reliability and lifetime of PV inverters considering the PV array sizing. The evaluation is based on the mission profile of the installation sites in Denmark and Arizona, where the reliability-critical components such as power devices and capacitors are considered. The results reveal that the variation in the PV array sizing can considerably deviate the reliability performance and lifetime expectation of PV inverters, especially for those installed in Denmark, where the average solar irradiance level is relatively low. In that case, a certain design margin in term of reliability is required to ensure high-reliable operation of PV inverters.**

***Index Terms*—PV inverters, lifetime, reliability, mission profile, PV arrays, oversizing, Monte Carlo analysis, cost of energy.**

I. Introduction

With the aim to introduce more renewable energy into the power system and due to the still declining cost of PV panels and installation, the PV industry has had a high growth rate in the last decades [1]. Nevertheless, in order to further increase the PV penetration level, the cost of PV energy has to be reduced even more to make the PV power plant comparable to the conventional energy (e.g., fossil fuel). It is recommended in [2] that the cost of PV energy (for residential applications in the US) has to be reduced from 0.18 USD/kWh in 2016 to 0.05 USD/kWh by 2030. This is a challenging target to reduce the PV energy cost by more than 3 times in the near future. There are several ways to reduce the cost of PV energy and achieve the above target (e.g., by improving efficiency and enhancing lifetime). Among others, one commonly (and practically) used solution is to oversize the PV arrays (the cost of PV modules is relatively low), where the rated power of the PV arrays is intentionally designed to be higher than the rated power of the PV inverter [3]–[5], as it is shown in Fig. 1. By doing so, the PV inverter will operate close to its rated power during a larger proportion of time, and thus more PV energy can be captured during the non-peak production periods. As the PV panel cost is still declining, where the PV module price drops around 13% per year [6], oversizing the PV arrays is currently an attractive and reasonable solution with a minor increase in the system cost using current technologies [7]–[9].

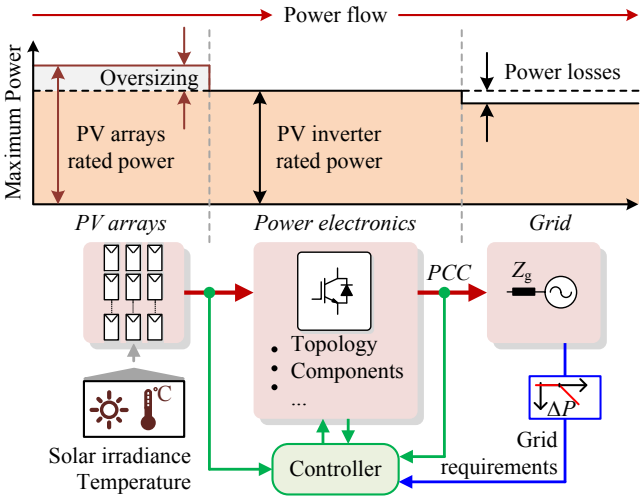

Fig. 1. Maximum power delivery at different power conversion stages of grid-connected PV systems with oversized PV arrays.

The PV power extraction during a day with oversized PV arrays is illustrated in Fig. 2, where the overall energy production is increased due to the higher energy yield under low solar irradiance conditions. Nevertheless, the oversizing will affect the PV inverter operation, which is a link between the PV arrays and the grid. Impacts of the PV array oversizing on the cost of PV energy and design approaches to maximize the energy yield have been addressed in literature. In [10], the impact of the PV array sizing on the energy cost is discussed for different system topologies. A similar study has been carried out in [11]–[13], where several installation sites (with different climate conditions) are considered. Optimum design solutions for oversizing the PV arrays have been proposed in

Manuscript received October 18, 2017; revised January 26, 2018; accepted March 26, 2018. Paper 2017-SECSC-1173.R1, presented at the 9th Annual IEEE Energy Conversion Congress & Exposition, Cincinnati, Ohio, October 1-5, 2017, and approved for publication in the IEEE Transactions on Industry Application by the Sustainable Energy Conversion Systems Committee of the IEEE Industry Applications Society. This work was supported by Innovation Fund Denmark through the Advanced Power Electronic Technology and Tools (APETT) project.

The authors are with the Department of Energy Technology, Aalborg University, DK-9220 Aalborg, Denmark (e-mail: ars@et.aau.dk; yoy@et.aau.dk; des@et.aau.dk; fbl@et.aau.dk; zda@et.aau.dk).

This article has been accepted for publication in a future issue of this journal, but has not been fully edited. Content may change prior to final publication. Citation information: DOI 10.1109/TIA.2018.2825955, IEEE Transactions on Industry Applications

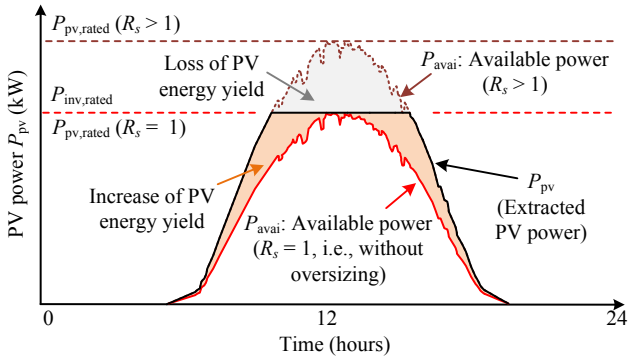

Fig. 2. PV power extraction with oversized PV arrays (P_{avai}: available PV power, P_{pv}: extracted PV power, $P_{pv,rated}$: PV array rated power, $P_{inv,rated}$: PV inverter rated power, $R_s = P_{pv,rated}/P_{inv,rated}$: sizing ratio).

[14]–[17] with the aim to maximize the PV energy yield while minimizing the system cost due to the oversizing.

Nevertheless, the prior-art discussions did not consider the impact of oversizing the PV arrays on the inverter reliability and lifetime. In other words, it is normally assumed that the PV inverter lifetime remains the same regardless of the PV array sizing. However, oversizing the PV array will inevitably affect the operation and the loading, and thus the inverter reliability and lifetime. For instance, the PV inverters with oversized PV arrays will have longer operating time at high power production than those without oversized PV arrays under the same mission profile (i.e., solar irradiance and ambient temperature) following Fig. 2. This will increase the thermal stresses of the critical components (e.g., power devices and capacitors), challenging their reliability. As the cost associated with the PV inverter failure is around 59% of the total system cost, the PV inverter lifetime plays a crucial role in the entire system cost assessment [18]–[21]. In that case, the increased operational and maintenance cost of the PV inverter due to oversizing may counteract the benefits of the increased energy production, resulting in a negative impact on the overall PV energy cost [22]. This issue has been pointed out in [8] and [13], but detailed lifetime analysis has not been addressed yet and thus its impact on the PV inverter reliability has not been quantified. More importantly, the sizing ratio (which indicates the degree of oversizing) also varies with the installation site. In that case, the variation in the PV array sizing ratio may impose a deviation in the reliability performance and lifetime expectation of the PV inverter, which needs to be quantified in order to ensure high-reliable operation of the designed PV inverter. This information can be used to identify a required design margin of the PV inverter in terms of reliability.

To fill in this gap, this paper investigates the impacts of the PV array sizing on the PV inverter reliability and lifetime. The analysis includes a lifetime evaluation of reliability-critical components in the system such as power devices and capacitors, where the system-level reliability assessment is performed considering the component-level reliability. This is an extension of the previous work in [23]. The lifetime evaluation is carried out with a case study of the installation

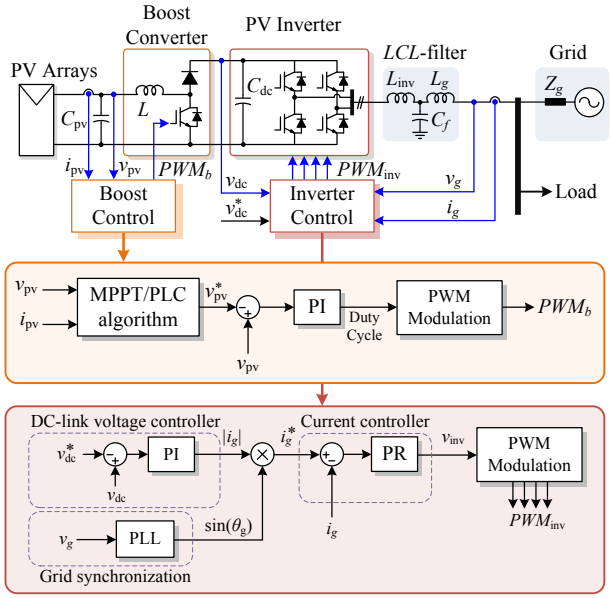

Fig. 3. System configuration and control structure of a two-stage single-phase grid-connected PV system (MPPT - Maximum Power Point Tracking, PLC - Power Limiting Control, PI - Proportional Integral, PR - Proportional Resonant, PLL - Phase-Locked Loop, PWM - Pulse Width Modulation).

sites in Denmark and Arizona, which is described in § II. A mission profile-based lifetime evaluation of the PV inverter is presented in § III, and it is applied to the case study as discussed in § IV. Then, the reliability assessment based on the Monte Carlo simulation together with the reliability block diagram of the system (i.e., the PV inverter) is carried out in § V to obtain the system-level reliability performance. Finally, concluding remarks are given in § VI.

II. Case Study Description

A. System Description

The system configuration and control structure of a single-phase grid-connected PV system are shown in Fig. 3. Here, a two-stage configuration is adopted, where two power converters—a boost dc-dc converter and a full-bridge dc-ac inverter (i.e., the PV inverter)—are employed as an interface between the PV arrays and the grid [24]. This two-stage configuration is widely used in residential/commercial PV systems (e.g., with the rated power of 1 kW - 30 kW), where the power extraction from the PV arrays is achieved by controlling the boost converter [25]. Nevertheless, the analysis discussed in this paper can also be applied to other system topologies. Normally, a Maximum Power Point Tracking (MPPT) algorithm is implemented in the boost converter by regulating the PV voltage v_{pv} at the Maximum Power Point (MPP) to optimize the energy yield. However, in the case of oversized PV arrays, the extracted PV power P_{pv} cannot exceed the PV inverter rated power $P_{inv,rated}$ for safety (e.g., to ensure that the components are operated within the safe operating area). In that case, the extracted PV power P_{pv} has to be limited at the PV inverter rated power level (i.e., $P_{pv} = P_{inv,rated}$), which is achieved by regulating the PV power

This article has been accepted for publication in a future issue of this journal, but has not been fully edited. Content may change prior to final publication. Citation information: DOI 10.1109/TIA.2018.2825955, IEEE Transactions on Industry Applications

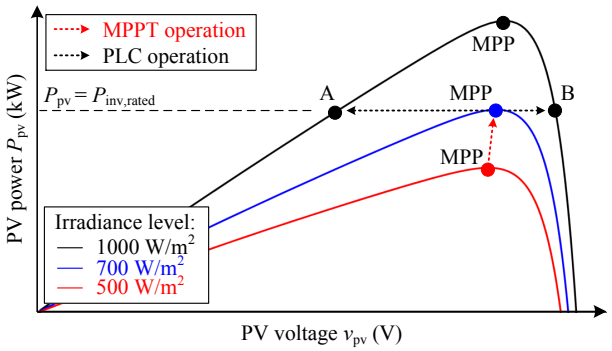

Fig. 4. Operational principle of the PV system with oversized PV arrays under the Maximum Power Point Tracking (MPPT) operation, e.g., operating at the Maximum Power Point (MPP), and Power Limiting Control (PLC) operation, e.g., operating at A or B.

below the MPP [3]. At the grid-side, the PV inverter delivers the extracted power to the ac grid by regulating the dc-link voltage v_{dc} to be constant, which is achieved through the control of the grid current i_g. Additionally, a Phase-Locked Loop (PLL) is also implemented for synchronization [26].

B. Operational Principle with Oversized PV Arrays

It is very common to define the sizing ratio R_s as the ratio of the PV array rated power at the Standard Test Condition (STC), $P_{\text{pv,rated}}$, over the PV inverter rated power $P_{\text{inv,rated}}$:

$$R_s = \frac{P_{\text{pv,rated}}}{P_{\text{inv,rated}}} \tag{1}$$

Usually, the PV system is oversized (i.e., $R_s > 1$) in order to capture more PV energy (e.g., under weak solar irradiance conditions) and increase the PV inverter utilization [9]. However, due to the oversizing, the available PV power of the oversized PV arrays can be higher than the rated power of the PV inverter (e.g., during the peak power generation periods). In that case, the extracted PV power has to be curtailed at the rated inverter power level, which is achieved by moving the operating point of the PV array away from the MPP as shown in Fig. 4 (either at A or B) [27]. This operation is referred to as the Power Limiting Control (PLC) in this paper. Notably, this will inevitably result in the loss of PV energy yield due to the power limitation, i.e., a negative impact on the cost of energy. Thus, the sizing ratio should be optimally designed considering the system cost (e.g., PV panels and inverters) and the solar resource (e.g., the irradiance level) of the installation sites [14]–[17]. Accordingly, the sizing ratio varies with the installation sites, where the typical value is in the range of $1 \leq R_s \leq 1.5$ [9].

C. Mission Profile of the PV Systems

A mission profile is a representation of the operating condition of the system [28]. The solar irradiance and ambient temperature are considered as mission profiles of the PV systems, since the PV power production is strongly dependent on the two parameters. The one-year mission profiles recorded

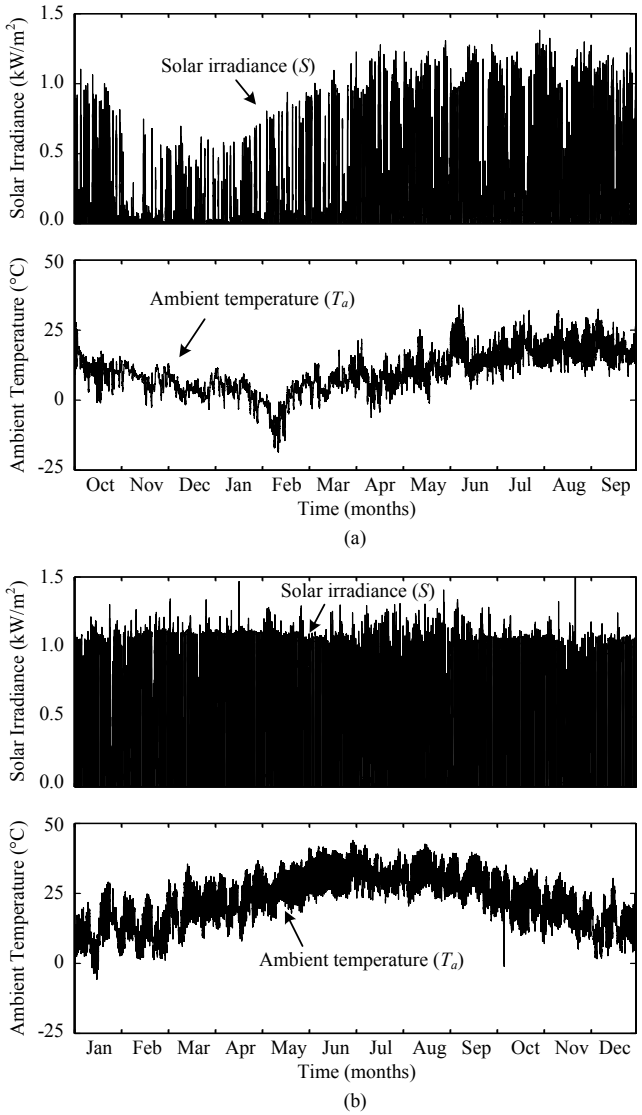

Fig. 5. Yearly mission profiles (i.e., irradiance and ambient temperature with a sampling rate of 5 mins per sample) in: (a) Denmark and (b) Arizona.

in Denmark and Arizona with a sampling rate of 5 minutes per sample are used in this study, as shown in Fig. 5. From the recorded mission profiles in Arizona, the average solar irradiance level is constantly high through the year. This is in contrast with the mission profile in Denmark, where the average solar irradiance level is relatively low through November to February. Additionally, the ambient temperature in Denmark also varies in a wide range with the minimum being around -18 °C during winter. The impact of oversizing the PV arrays on the lifetime of the inverters installed at the two sites will be different due to the mission profile characteristics, which will be demonstrated later in this paper.

III. Mission Profile-based Lifetime Estimation

The lifetime of PV inverters can be considerably influenced by the operating condition of the system, i.e., mission profiles [31]. For instance, the PV power production is mainly

This article has been accepted for publication in a future issue of this journal, but has not been fully edited. Content may change prior to final publication. Citation information: DOI 10.1109/TIA.2018.2825955, IEEE Transactions on Industry Applications

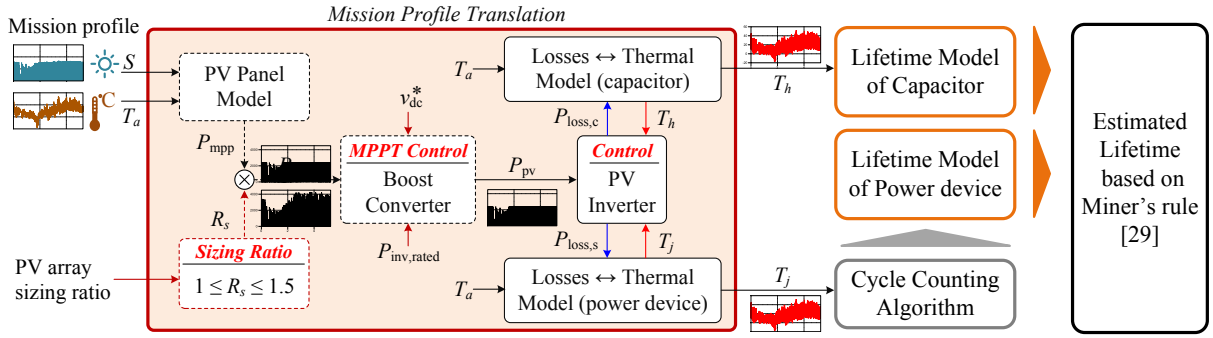

Fig. 6. Mission profile-translation diagram of a single-phase PV system, where the PV array sizing ratio R_s is considered [29], [30].

determined by the solar irradiance and ambient temperature conditions of the system, and it will eventually be translated into the thermal stress of the PV inverter. For some reliability-critical components in the PV inverter (e.g., power devices and capacitors), this thermal stress can lead to wear-out failures, e.g., bond wire lift-off of power devices after a given number of thermal cycles [32]. Therefore, the mission profile is normally considered in the lifetime evaluation, in which three main tasks are involved [29], [30], [33]–[37]: 1) Mission profile translation to thermal loading, 2) Thermal cycling interpretation, and 3) Lifetime modeling of components. The flow diagram of this procedure is summarized in Fig. 6, and will be elaborated as follows.

A. Mission Profile Translation to Thermal Loading

First, the mission profile should be translated into the thermal loading of the reliability-critical components in the system (e.g., power devices and capacitors). For given solar irradiance and ambient temperature profiles, the PV power at the MPP of the PV array, P_{mpp}, can be determined by using the PV panel characteristic model [38]. In this case, the PV panel model with the same rated power as the PV inverter is considered (representing the case with non-oversized PV arrays). Then, the available PV power P_{avai} can be calculated by multiplying the PV power at the MPP, P_{mpp}, with the sizing ratio, R_s [23]. This implies that the actual available PV power can be higher than the PV inverter rated power with oversized PV arrays (i.e., $R_s > 1$). Afterwards, the extracted PV power P_{pv} (i.e., input power of the PV inverter) is obtained considering the MPPT operation efficiency (99%) and the maximum extracted PV power is limited to the PV inverter rated power.

Then, considering the PV inverter efficiency, the power losses dissipated in the power devices, $P_{\text{loss,s}}$, can be obtained and applied to the thermal model of the power devices. By doing so, the junction temperature profile of the power device, T_j, during operation is obtained. Similarly, the power losses dissipated in the capacitor, $P_{\text{loss,c}}$, can be determined considering the ripple current in the dc-link and the Equivalent Series Resistance (ESR) of the capacitor [36]. Afterwards, the hotspot temperature of the capacitor, T_h, is calculated with the power losses $P_{\text{loss,c}}$. A detailed discussion regarding the mission profile translation of the power device and capacitor can be found in [29], [34], [35] and [30], [36], [37], respectively. Normally, a Look-Up Table (LUT) generated from the conduction and switching losses of the power device and the thermal impedance given in the datasheet is employed to assist long-term simulations (e.g., one-year mission profiles) [29].

B. Thermal Cycling Interpretation

From the previous step, the thermal loading of the components in the PV inverter such as the junction temperature of the power device, T_j, and the hotspot temperature of the capacitors, T_h, can be obtained for a given mission profile. However, in the case of the power device, the main failure mechanism is related to the thermal cycling, e.g., resulting in a bond wire lift-off [28]. In that case, the information regarding the thermal cycling, e.g., the number of cycles n_i at a certain cycle amplitude ΔT_j, mean junction temperature T_{jm}, and cycle period t_{on} are required for lifetime estimation. The above information cannot be acquired directly from the junction temperature profile, as it usually contains the mission profile dynamics (i.e., irregular).

In order to apply such an irregular junction temperature profile to the lifetime model, which is based on the empirical data, a cycle counting algorithm is needed for the thermal cycling interpretation [34]. This method has been widely used in the lifetime and stress analysis related to the thermal cycling. For instance, a rainflow counting algorithm can be employed to decompose the irregular profile into several regular cycles according to the cycle amplitude, its average value, and the cycle period. By applying this method to the device junction temperature profile, the number of cycles n_i at a certain cycle amplitude ΔT_j, mean junction temperature T_{jm}, and cycle period t_{on} can be obtained. The information can be directly applied to the lifetime model and the lifetime of the power device can then be evaluated.

C. Lifetime Model of the Components

According to the field experiences, there are several components (e.g., power devices, capacitors, gate drivers, fans, and etc.) that induce failures in the PV inverters [19]. In fact, the failure mechanism of each components may have a cross-effect on the reliability of other components in the system, leading

TABLE I
PARAMETERS OF THE LIFETIME MODEL OF AN IGBT MODULE [40].

Parameter	Value	Experimental condition
A	3.4368×10^{14}	
α	-4.923	$64\ \text{K} \leq \Delta T_j \leq 113\ \text{K}$
β_1	-9.012×10^{-3}	
β_0	1.942	$0.19 \leq ar \leq 0.42$
C	1.434	
γ	-1.208	$0.07\ \text{s} \leq t_{on} \leq 63\ \text{s}$
f_d	0.6204	
E_a	0.06606 eV	$32.5\ ^\circ\text{C} \leq T_j \leq 122\ ^\circ\text{C}$
k_B	8.6173324×10^{-5} eV/K	

to very complicated analysis. In this paper, only the wear-out failure mechanism of the power devices and capacitors, which are reported to be the main life-limiting components of the PV inverter [39], are considered for simplicity.

1) Lifetime Model of the Power Devices: For the power device (e.g., IGBT), one main failure mechanism is related to the thermal cycling, whose lifetime model is given as

$$N_f = A \times (\Delta T_j)^{\alpha} \times (ar)^{\beta_1 \Delta T_j + \beta_0} \times \left[\frac{C+(t_{on})^{\gamma}}{C+1}\right] \times \exp\left(\frac{E_a}{k_b \times T_{jm}}\right) \times f_d \quad (2)$$

where N_f is the number of cycles to failure [40]. The mean junction temperature T_{jm}, cycle amplitude ΔT_j, and cycle period t_{on} are the stress level obtained from the cycle counting algorithm, while the other parameters are given in Table I.

By using the Miner's rule [34], the Life Consumption (LC) or damage of the power device, can be calculated as [34]

$$LC = \sum_i \frac{n_i}{N_{fi}} \quad (3)$$

where n_i is the number of cycles (obtained from the rainflow analysis) for a certain T_{jm}, ΔT_j, and t_{on}, and N_{fi} is the number of cycles to failure calculated from (2) at that specific stress condition.

2) Lifetime Model of the Capacitors: In the case of the capacitors, the main stress parameters are the hotspot temperature T_h and the operating voltage of the capacitor V_{op}. The lifetime model of the capacitor is given as

$$L_f = L_m \times \left(4.3 - 3.3\frac{V_{\text{op}}}{V_{\text{rated}}}\right) \times 2^{\left(\frac{T_m - T_h}{10}\right)} \quad (4)$$

in which L_f is the time-to-failure under the thermal stress level of T_h and the voltage stress level of V_{op} [41], and the other parameters are given in Table II [42]. Notably, the impact of the voltage stress can be neglected when the voltage stress is below the rated voltage (e.g., $V_{\text{op}} \leq V_{\text{rated}}$) [41]. In that case, only the thermal stress has the influence on the operating life of the capacitors, and the lifetime model can be simplified as

$$L_f = L_m \times 2^{\left(\frac{T_m - T_h}{10}\right)} \quad (5)$$

Then, the Miner's rule [34] can be applied, and the LC of the capacitor can be determined as

$$LC = \sum_i \frac{l_i}{L_{fi}} \quad (6)$$

TABLE II
PARAMETERS OF THE LIFETIME MODEL OF A CAPACITOR [42].

Parameter	Symbol	Value
Rated lifetime (at V_{rated} and T_m)	L_m	3000 hours
Rated operating voltage	V_{rated}	350 V
Rated operating temperature	T_m	105°C

TABLE III
PARAMETERS OF THE TWO-STAGE SINGLE-PHASE PV SYSTEM (FIG. 3).

PV array rated power	6 kW (with sizing ratio R_s = 1)
PV inverter rated power	6 kW
Boost converter inductor	L = 1.8 mH
DC-link capacitance	C_{dc} = 1100 μF (Two capacitors of 2200 μF/ 350V connected in series)
LCL-filter	L_{inv} = 4.8 mH, L_{g} = 2 mH, C_f = 4.3 μF
Switching frequency	Boost converter: f_b = 16 kHz, Full-Bridge inverter: f_{inv} = 8 kHz
DC-link voltage	v_{dc}^* = 450 V
Grid nominal voltage (RMS)	V_g = 230 V
Grid nominal frequency	$\omega_0 = 2\pi \times 50$ rad/s

where l_i is the operating time for a set of T_h and V_{op} (e.g., the mission profile time resolution), and L_{fi} is the time-to-failure calculated from (5) at that specific stress condition.

The LC is an indicator of how much lifetime of the component is consumed (or damaged) during the operation (e.g., according to the applied mission profile) [28]. For example, the LC calculated from a one-year mission profile will represent a yearly LC of the component (e.g., the power devices, capacitors). When the LC is accumulated to unity (e.g., after several years of operation), the component is considered to reach its end of life, and the lifetime can be predicted.

IV. LIFETIME EVALUATION (CASE STUDY)

In this section, the lifetime evaluation discussed in § III is applied to the two-stage PV system in Fig. 3 with the parameters shown in Table III. The 600V/50A Insulated-Gate Bipolar Transistor (IGBT) devices from a leading manufacturer [43] are used, while the cooling system (e.g., heat sink sizing) is designed to ensure the maximum junction temperature below 100 °C at the rated operating condition (e.g., ensuring the operation within safe operating area). The dc-link consists of two aluminum electrolytic capacitors with the capacitance of 2200 μF and the rated voltage of 350 V [37], [42] connected in series to achieve the required dc-link capacitance (i.e., C_{dc} = 1100 μF) and voltage capability. The case study is based on the mission profiles in Denmark and Arizona (see Fig. 5) with different sizing ratios. The thermal loading of the power device and capacitor and their corresponding LC are evaluated.

A. Thermal Loading of PV Inverters

The thermal loading of the power devices (i.e., the mean junction temperature T_{jm} and the cycle amplitude ΔT_j) and the capacitors (i.e., the hotspot temperature T_h) in the PV inverter installed in Denmark and Arizona are shown in Figs.

This article has been accepted for publication in a future issue of this journal, but has not been fully edited. Content may change prior to final publication. Citation information: DOI 10.1109/TIA.2018.2825955, IEEE Transactions on Industry Applications

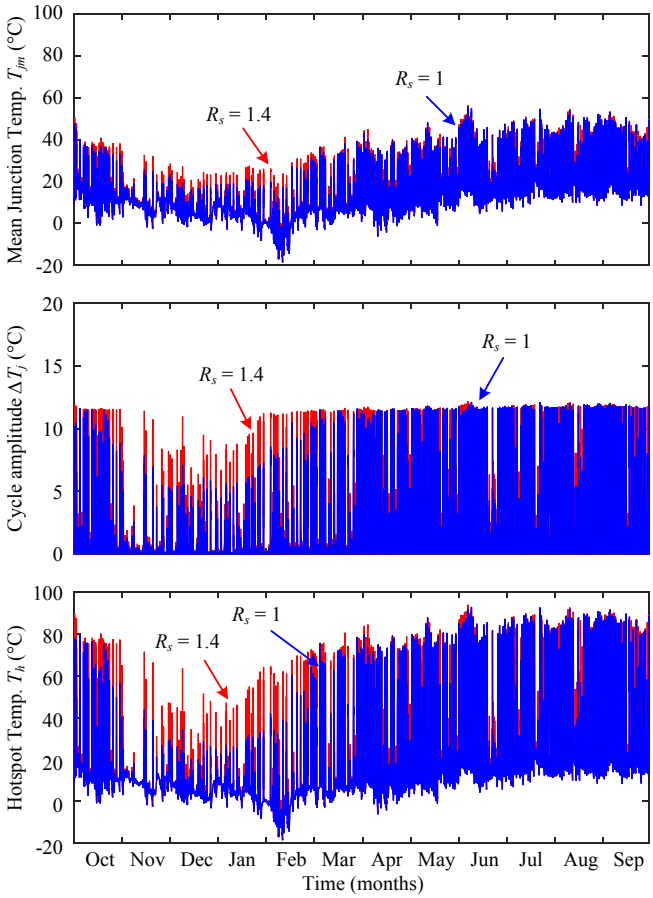

Fig. 7. Mean junction temperature T_{jm}, cycle amplitude ΔT_j of the power device, and hotspot temperature of the capacitor T_h under a mission profile in Denmark with two sizing ratios (blue plot: $R_s = 1$, red plot: $R_s = 1.4$).

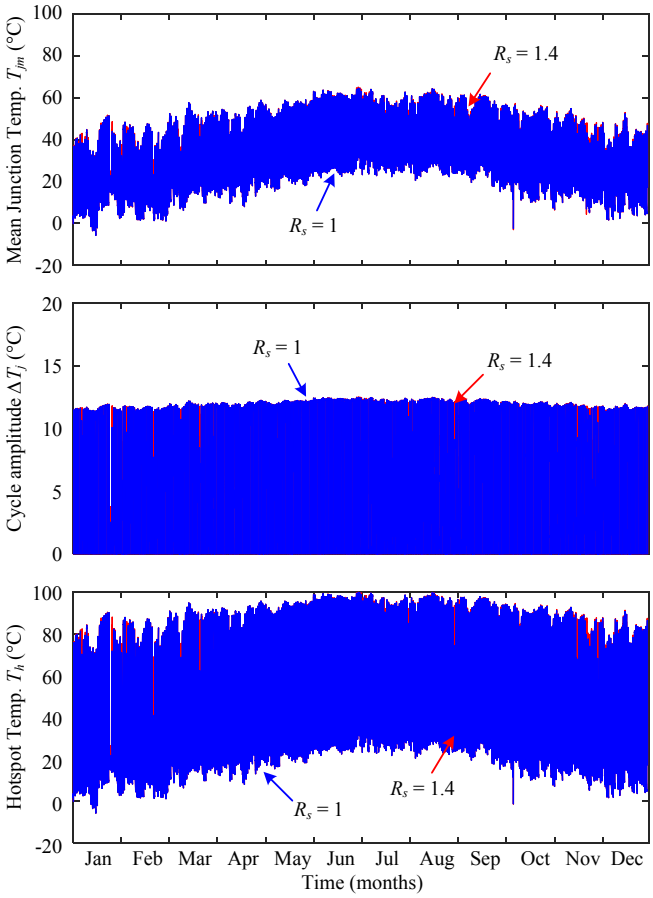

Fig. 8. Mean junction temperature T_{jm}, cycle amplitude ΔT_j of the power device, and hotspot temperature of the capacitor T_h under a mission profile in Arizona with two sizing ratios (blue plot: $R_s = 1$, red plot: $R_s = 1.4$).

7 and 8, respectively. Two cases with $R_s = 1$ (i.e., non-oversized PV arrays) and $R_s = 1.4$ (i.e., oversized PV arrays) are considered. It can be seen from Fig. 7 that the PV inverter installed in Denmark with oversized PV arrays (i.e., $R_s = 1.4$) has a strong increase in the thermal loading compared to the case where $R_s = 1$, especially during November through February (when the solar irradiance level is low). The impact of oversizing PV arrays is less pronounced with the PV system installed in Arizona, where only a small increase in the thermal loading of the PV inverter is observed in Fig. 8. This is due to the fact that the PV inverter installed in Arizona with $R_s = 1.4$ mostly operates in the power limiting mode (i.e., $P_{\text{pv}} = P_{\text{inv,rated}}$) because of the high average solar irradiance level through the year. In that case, oversizing the PV array will not significantly increase the PV power production and thus the thermal loading of the components in the inverter.

B. Lifetime Evaluation

From the thermal loading of the power device (i.e., mean junction temperature T_{jm} and cycle amplitude ΔT_j) in Figs. 7 and 8, the corresponding LC of the power device during one-year operation can be calculated following (3). A similar approach can also be applied to determine the LC of the capacitor based on the hotspot temperature T_h (in Figs. 7 and 8) following (6). The normalized LC (compared with the case without oversizing) of the power devices and capacitor of the PV inverter with different sizing ratios (e.g., $1 \leq R_s \leq 2$) under the mission profile in Denmark and Arizona are shown in Figs. 9 and 10, respectively. This parameter indicates a relative change in the LC due to the sizing ratio, and gives a comparison of the sizing ratio impacts for different mission profiles in term of deviation in the reliability performance and lifetime expectation.

As it is expected, the impact of oversizing on the LC is significant with the mission profile in Denmark, where the LC increases considerably as R_s increases (see Fig. 9). Notably, the higher LC results in shorter lifetime of the PV inverter. In contrast, the LC of the PV inverter installed in Arizona is less affected by the sizing ratio of the PV arrays (see Fig. 10). In this case, the LC only increases slightly, and it saturates around 1.5 times of the initial LC (i.e., LC without oversizing) for the power device and 1.4 times of the initial LC for the capacitor. This is simply due to the mission profile characteristics (especially the solar irradiance profile) in Denmark, where the average irradiance level is relatively low during the winter. By oversizing the PV arrays, the PV power production during the winter is increased considerably without reaching the rated PV inverter power limit. On the other hand,

This article has been accepted for publication in a future issue of this journal, but has not been fully edited. Content may change prior to final publication. Citation information: DOI 10.1109/TIA.2018.2825955, IEEE Transactions on Industry Applications

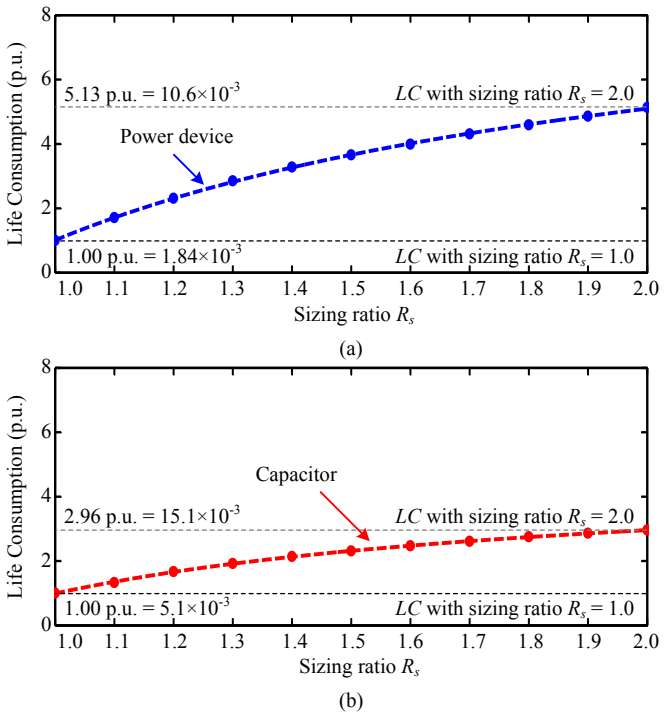

Fig. 9. Normalized life consumption of components in PV inverters with different sizing ratios R_s for the mission profile in Denmark: (a) power device and (b) capacitor.

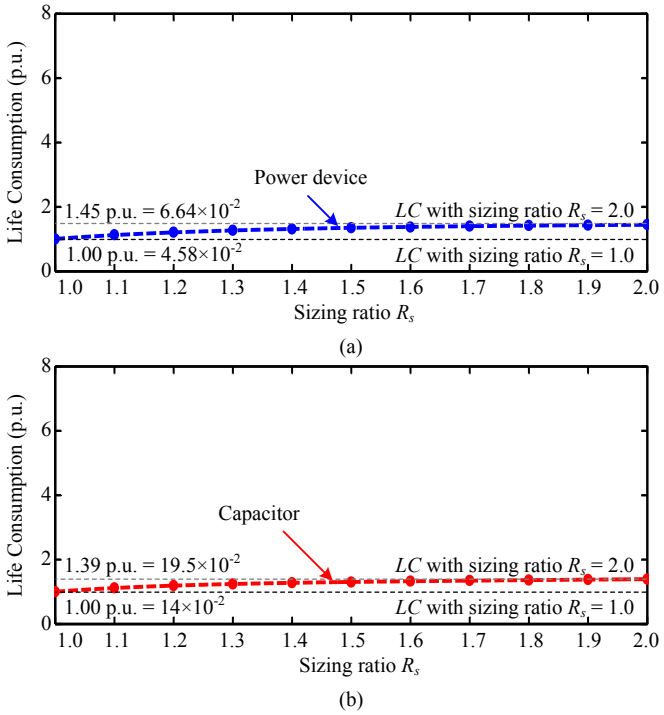

Fig. 10. Normalized life consumption of components in PV inverters with different sizing ratios R_s for the mission profile in Arizona: (a) power device and (b) capacitor.

the solar irradiance in Arizona is relatively high throughout the year. Thus, oversizing the PV arrays can easily lead to a power limiting operation, due to the maximum capability of the PV inverter. As a consequence, only a small increase in the PV power production is obtained, and thus the impact on the LC of the PV inverter is less significant compared to that in Denmark. The above results indicate that the reliability of the PV inverters (e.g., power devices) installed in Denmark can be deviated significantly as the PV array is oversized.

Notably, the absolute value of the LC of the inverter installed the Arizona is much higher than that in Denmark, e.g., more than 10 times, due to the mission profile characteristics (i.e., the solar irradiance resource). In that case, the PV inverter in Arizona will have shorter lifetime even without oversizing the PV array. The above discussion only compares the influence of the sizing ratio in a relative way (e.g., by normalizing the LC with the case without oversizing).

V. Reliability Analysis

From the previous lifetime evaluation, the LC during one-year operation of each individual component can be calculated from the mission profile. In practice, there are uncertainties in the lifetime prediction introduced by, e.g., the manufacturing process, the mission profile, and the lifetime model parameters. In order to evaluate the reliability of the entire system, these uncertainties are considered during the lifetime evaluation process by means of Monte Carlo simulations [44]–[48], where parameter variations (e.g., lifetime model and the stress parameters) are introduced to represent the uncertainties. By doing so, the lifetime distribution and the unreliability function of the components in the system (e.g., power device and capacitor) can be expressed in terms of statistical values. Moreover, for the system with several components (e.g., the PV inverter in Fig. 3), the reliability of the system can be obtained from the component-level reliability by using the reliability block diagram [44]–[46]. This procedure will be demonstrated with the case study based on the previously discussed mission profile and sizing ratio.

A. Monte Carlo Simulation (Component-Level)

The overall process of the Monte Carlo-based reliability assessment is shown in Fig. 11. The basic idea of this method is to model the parameters used in the calculation (e.g., lifetime model and stress parameters) with a certain distribution function, instead of using fixed parameters. For instance, the parameters of the lifetime model in Table I & II can be modeled with a certain distribution with a range of variations (e.g., normal distribution with 5% parameter variation). In this way, the parameter variations can be introduced in the calculation in order to represent uncertainties in practical applications. Then, the lifetime evaluation (following the approach in § III) is carried out with a population of n samples. By doing so, the lifetime distribution (e.g., the Weibull distribution) of the power device $f(x)$ can be constructed from the lifetime yield (i.e., $1/LC$) of n samples.

An example of the results obtained from the Monte Carlo simulation with the population of 10000 samples (e.g., n = 10000) is illustrated in Fig. 12. It can be seen from the lifetime distribution of the power device $f_s(t)$ and capacitor $f_c(t)$ in Fig. 12(a) that most of the population fail after 18 years of

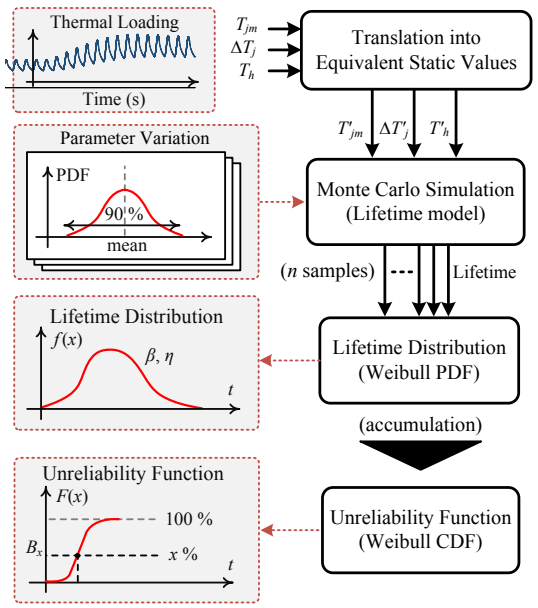

Fig. 11. Flow diagram of the Monte Carlo-based reliability assessment of components in PV inverters (PDF: Probability Density Function, CDF: Cumulative Density Function) [46].

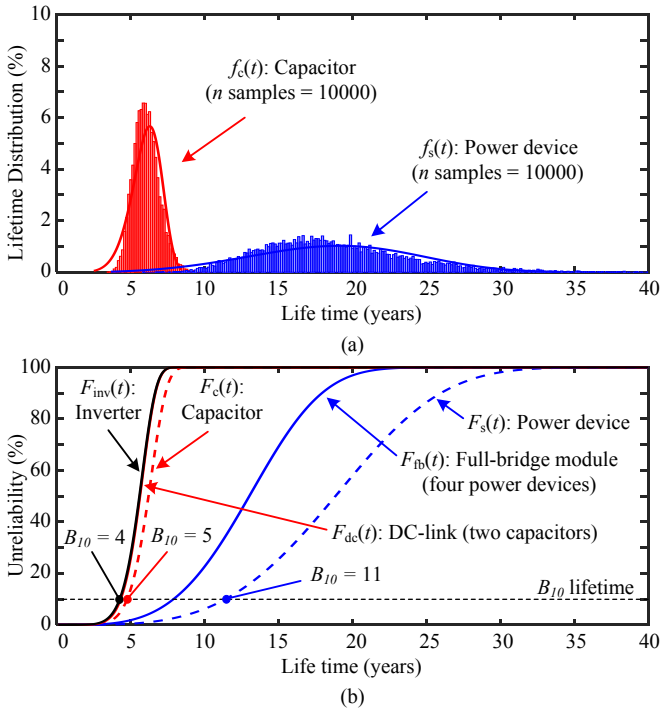

Fig. 12. Results from the Monte Carlo simulation with 10000 samples of the PV inverter with a sizing ratio of R_s = 1.2 for the mission profile in Arizona: (a) lifetime distribution of power devices and capacitors in the PV inverter and (b) unreliability function of component-level (i.e., power device and capacitor), sub-system-level (i.e., full-bridge module and dc-link), and system-level (i.e., inverter) in the PV inverter.

operation in the case of power device and 6 years of operation in the case of capacitors (with the sizing ratio R_s = 1.2 in Arizona).

From the lifetime distribution of the component, it is also possible to obtain the component unreliability function $F(x)$, which is a cumulative function of the lifetime distribution [49]. The unreliability function can be used to indicate the development of failure overtime. For instance, the time when $x\%$ of a population is failed can be obtained from the unreliability function, and it is normally referred to as the B_x lifetime. This quantity can be used as a reliability metric which contains a statistical information of the failure rate. Based on the results in Fig. 12(a), the unreliability function of the power device $F_s(t)$ and the capacitor $F_c(t)$ can be constructed as it is shown in Fig. 12(b), where the B_{10} lifetime of each component is also indicated.

B. Reliability Block Diagram (System-Level)

From the previous analysis, the reliability (or unreliability) of each individual component in the system can be obtained. For the system with several components (e.g., the PV inverter with several power devices and capacitors), the reliability of the entire system can be assessed by using the reliability block diagram, which represents the reliability interaction among components in the system [48]–[50].

For the system with n components and a single failure of any component will cause the overall system to fail, the system is considered as a series connection of the reliability block diagram, as it is illustrated in Fig. 13(a). Following the reliability block diagram approach [50], the unreliability of the entire system $F_{\text{sys}}(t)$ can be calculated as

$$F_{\text{sys}}(t) = 1 - \prod_{i=1}^{n}(1 - F_i(t)) \tag{7}$$

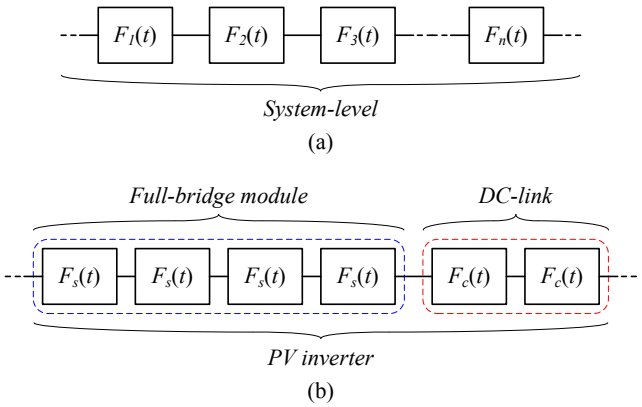

Fig. 13. Series connection of reliability block diagram of: (a) system with n components and (b) PV inverter with full-bridge module and dc-link ($F_s(t)$: unreliability of the power device, $F_c(t)$: unreliability of the capacitor).

where $F_i(t)$ is the unreliability of the i-th component in the system.

For the PV inverter used in this study (see Fig. 3), the system consists of two main sub-systems: the full-bridge module and the dc-link. The full-bridge module consists of four power devices, while the dc-link consists of two capacitors connected in series. In this case, a failure of any power device will lead to a malfunction of the full-bridge power module. Similarly, a failure of a single capacitor will lead to a failure of the dc-link. Following the above consideration, the reliability block

This article has been accepted for publication in a future issue of this journal, but has not been fully edited. Content may change prior to final publication. Citation information: DOI 10.1109/TIA.2018.2825955, IEEE Transactions on Industry Applications

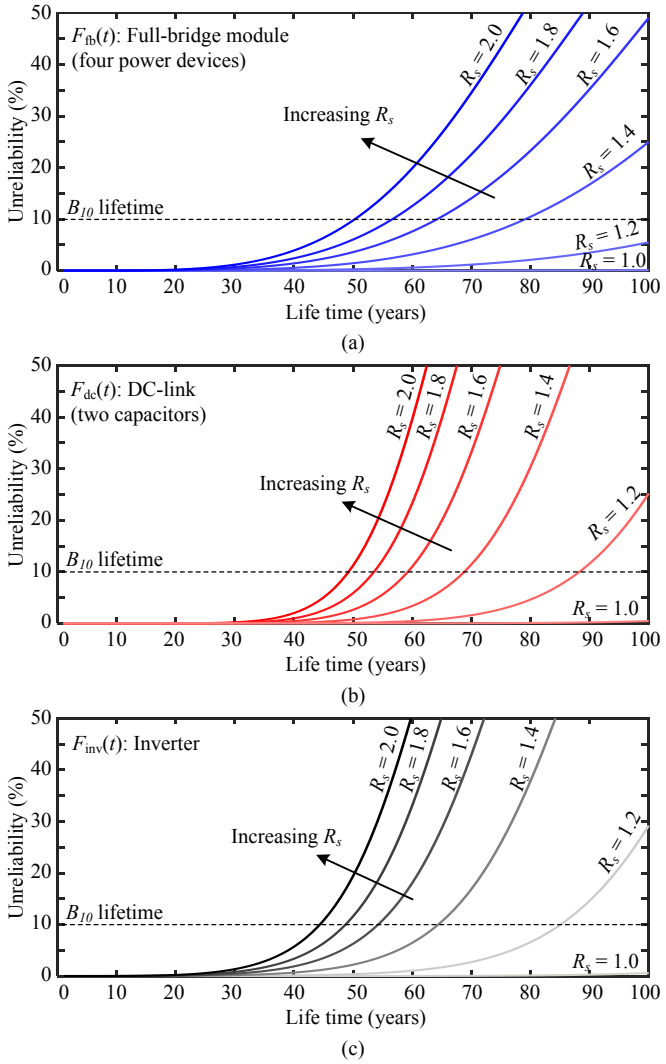

Fig. 14. Unreliability function of the PV inverter with different sizing ratios for the mission profiles in Denmark: (a) the full-bridge module (i.e., four power devices), (b) the dc-link (i.e., two capacitors), and (c) the inverter.

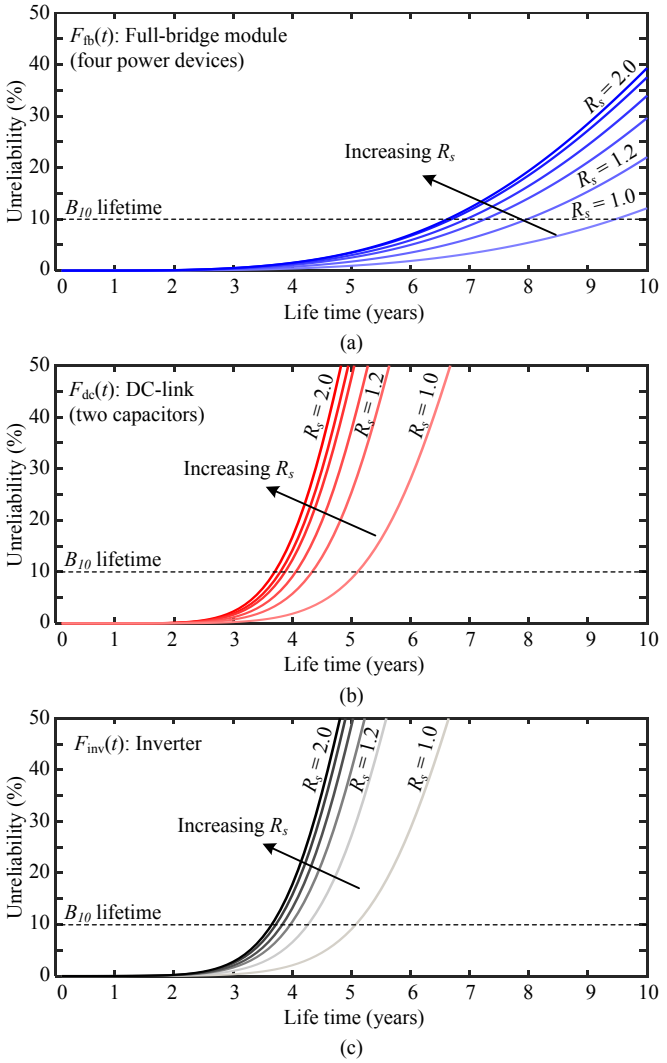

Fig. 15. Unreliability function of the PV inverter with different sizing ratios for the mission profiles in Arizona: (a) the full-bridge module (i.e., four power devices), (b) the dc-link (i.e., two capacitors), and (c) the inverter.

diagram of the entire PV inverter can be constructed based on a series connection, as it is shown in Fig. 13(b), and the unreliability of the PV inverter $F_{\text{inv}}(t)$ (e.g., system-level) can be calculated as

$$F_{\text{inv}}(t) = 1 - (1 - F_{\text{fb}}(t))(1 - F_{\text{dc}}(t)) \tag{8}$$

with

$$F_{\text{fb}}(t) = 1 - (1 - F_{\text{s}}(t))^4, \quad F_{\text{dc}}(t) = 1 - (1 - F_{\text{c}}(t))^2 \tag{9}$$

where $F_{\text{fb}}(t)$ is the unreliability of the full-bridge module (i.e., four power devices) and $F_{\text{dc}}(t)$ is the unreliability of the dc-link (i.e., two capacitors). An example of the system-level reliability assessment is demonstrated in Fig. 12(b), where the unreliability of the PV inverter is obtained by applying the reliability block diagram in Fig. 13(b). In this way, the system-level reliability assessment can be achieved from the component- and/or sub-system-level reliability.

C. Reliability Assessment (Case Study)

The reliability assessment of the PV inverter is carried out under two mission profiles: Denmark and Arizona. For each mission profile, the unreliability function of the components in the PV inverter (i.e., power device and capacitor) is calculated from the sample of 10000 population (i.e., n = 10000), where the parameter variation of 5% is introduced. Then, following the reliability block diagram approach in (8) and (9), the unreliability of the sub-system (i.e., the full-bridge module and the dc-link) and the entire system (i.e., the inverter) are obtained.

The impact of the sizing ratio R_s on the unreliability of the PV inverter under the mission profile in Denmark is shown in Fig. 14. It can be noticed from the unreliability function of the full-bridge module in Fig. 14(a) and the dc-link in Fig. 14(b) that the failure rate of the both sub-systems are comparable under the same sizing ratio. However, the failure rate of the dc-link is in general slightly higher than that of the full-bridge module. This implies that, in this case, the dc-link is the main

This article has been accepted for publication in a future issue of this journal, but has not been fully edited. Content may change prior to final publication. Citation information: DOI 10.1109/TIA.2018.2825955, IEEE Transactions on Industry Applications

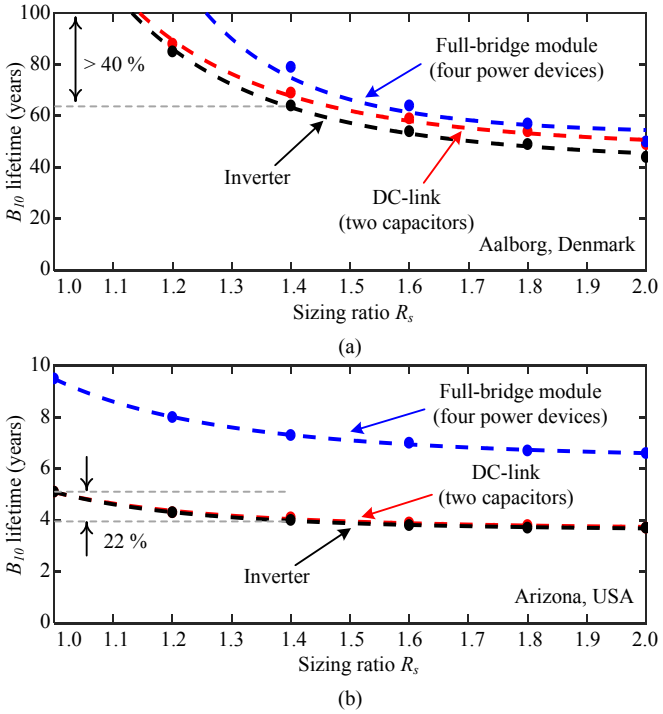

Fig. 16. B_{10} lifetime of the PV inverter and the sub-systems (i.e., full-bridge module and dc-link) with different sizing ratios for the mission profile in: (a) Denmark and (b) Arizona.

life-limiting sub-system in the PV inverter. Considering the impacts of the sizing ratio R_s, it can be seen from Fig. 14 that the failure rate of both the full-bridge module and the dc-link capacitors increases relatively fast with large sizing ratios. As a consequence, the failure rate of the entire PV inverter in Fig. 14(c) also increases significantly as the sizing ratio increases.

On the other hand, only a small change in the unreliability with different sizing ratios is observed under the mission profile in Arizona, as it is shown in Fig. 15. In this case, it can be seen that the failure rate of the full-bridge module and the dc-link in Figs. 15(a) and (b) are less affected by the sizing ratio, especially when the sizing ratio is higher than 1.4 (i.e., $R_s \geq 1.4$), compared to the case with the mission profile in Denmark. Moreover, the reliability of the dc-link is clearly more critical than the full-bridge module in this case, as it has a much higher failure rate under the same sizing ratio. This is mainly due to the high average ambient temperature in Arizona, which highly affects the lifetime of the capacitors.

From the unreliability function in Figs. 14 and 15, the B_{10} lifetime of the full-bridge module, the dc-link and the PV inverter with different sizing ratios can be obtained by considering the time when 10% of the population have failed, as it is also indicated in the same figure. This parameter is used as a reliability metric in this study. Notably, the B_{10} lifetime of the PV inverter with the mission profile in Denmark is higher than 50 years for the sizing ratio below 1.4 (i.e., $R_s \leq 1.4$), which is not practical (in general). In that case, other failure mechanisms or components will be dominant during this time period, and the B_{10} lifetime obtained from the thermal cycling related failure mechanism may not represent the main life-limiting factor of the PV inverter.

The B_{10} lifetime of the PV inverter with different sizing ratios for the two mission profiles is summarized in Fig. 16 to indicate the deviation in the PV inverter reliability under different PV array sizing ratios. It can be seen from the results that the B_{10} lifetime of the PV inverter in Denmark decreases considerably as the sizing ratio R_s increases. For instance, the B_{10} lifetime of the PV inverter decreases by more than 40 % when the sizing ratio of the PV system is increased from R_s = 1 to R_s = 1.4. This indicates that a certain design margin in terms of reliability is required for the PV inverter installed in Denmark to maintain its high-reliable operation under various PV array sizing ratios. In contrast, the impact of the sizing ratio R_s is less significant in the case of the mission profile in Arizona. For example, only a small reduction in the PV inverter lifetime is observed (i.e., around 22%) when the sizing ratio of the PV system is increased from R_s = 1 to R_s = 1.4. When the sizing ratio is further increased from R_s = 1.4 to R_s = 2, the B_{10} lifetime of the PV inverter remains almost constant. In this case, it can be clearly seen from the results in Fig. 16(b) that the dc-link is the critical part in the PV inverter. In order to improve the reliability of the overall system, the cooling system of the capacitor may need to be redesigned (e.g., using active cooling method). The above reliability assessment results are in agreement with the previous lifetime evaluation in § IV, where the impact of sizing ratio is less pronounced for the mission profile in Arizona due to the power limiting operation of the PV inverter. In that case, a small design margin is sufficient to ensure high-reliable operation of PV inverters with various PV array sizing ratios.

VI. Conclusion

The impact of the PV array sizing on the PV inverter reliability and lifetime has been investigated in this paper. A mission profile-based lifetime evaluation has been carried out on PV systems installed in Denmark and Arizona with different sizing ratios, where the lifetime of power devices and capacitors were considered. The evaluation showed a considerable impact of the PV array sizing on the reliability and lifetime of the PV inverter installed in Denmark, where the PV inverter thermal loading increases considerably with oversized PV arrays. In contrast, the increased loading because of the oversizing is less significant for the PV inverter installed in Arizona. This is mainly due to the average high irradiance condition through the year, where the PV inverter is almost always operating at the power limiting control when the PV arrays are oversized. Accordingly, the lifetime of the PV inverters installed in Denmark can decrease significantly with the large sizing ratio. In that case, a certain design margin in terms of reliability should be considered to ensure high-reliable operation of PV inverters under various PV array sizing ratios. Moreover, the operational and maintenance cost of the PV inverter should be carefully evaluated, as oversizing the PV arrays may result in a negative impact on the PV inverter reliability and thus the overall PV energy cost.

REFERENCES

[1] REN21, "Renewables 2017: Global Status Report (GRS)," 2017. [Online]. Available: http://www.ren21.net/.

[2] National Renewable Energy Laboratory, "On the path to sunshot: The role of advancements in solar photovoltaic efficiency, reliability, and costs," Tech. Rep. No. NREL/TP-6A20-65872, 2016.

[3] J. Fiorelli and M. Zuercher-Martinson, "How oversizing your array-to-inverter ratio can improve solar-power system performance," *Solar Power World*, vol. 7, pp. 42–48, 2013.

[4] T. Khatib, A. Mohamed, and K. Sopian, "A review of photovoltaic systems size optimization techniques," *Renew. Sustain. Energy Rev.*, vol. 22, pp. 454–465, 2013.

[5] M. Hussin, A. Omar, S. Shaari, and N. M. Sin, "Review of state-of-the-art: Inverter-to-array power ratio for thin-film sizing technique," *Renewable and Sustainable Energy Reviews*, vol. 74, pp. 265–277, 2017.

[6] Fraunhofer ISE, "Recent Facts about Photovoltaics in Germany," January 9, 2017. [Online]. Available: http://www.pv-fakten.de/.

[7] SMA, "7 reasons why you should oversize your PV array," Dec. 2015. [Online]. Available: http://en.sma-sunny.com/en/7-reasons-why-you-should-oversize-your-pv-array-2/

[8] Global Sustainable Energy Solutions (GSES) India, "Oversizing PV arrays," Tech. Rep., 2014.

[9] SolarEdge, "Oversizing of SolarEdge inverters, technical note," Tech. Rep., July 2016.

[10] F. He, Z. Zhao, and L. Yuan, "Impact of inverter configuration on energy cost of grid-connected photovoltaic systems," *Renewable Energy*, vol. 41, pp. 328–335, 2012.

[11] B. Burger and R. Ruther, "Site-dependent system performance and optimal inverter sizing of grid-connected PV systems," in *Proc. of PVSEC*, pp. 1675–1678, Jan. 2005.

[12] B. Burger and R. Ruther, "Inverter sizing of grid-connected photovoltaic systems in the light of local solar resource distribution characteristics and temperature," *Solar Energy*, vol. 80, no. 1, pp. 32–45, 2006.

[13] J. Good and J. X. Johnson, "Impact of inverter loading ratio on solar photovoltaic system performance," *Applied Energy*, vol. 177, pp. 475–486, Sep. 2016.

[14] J. D. Mondol, Y. G. Yohanis, and B. Norton, "Optimal sizing of array and inverter for grid-connected photovoltaic systems," *Solar Energy*, vol. 80, no. 12, pp. 1517–1539, Dec. 2006.

[15] S. Chen, P. Li, D. Brady, and B. Lehman, "Determining the optimum grid-connected photovoltaic inverter size," *Solar Energy*, vol. 87, pp. 96–116, 2013.

[16] R. Mounetou, I. B. Alcantara, A. Incalza, J. Justiniano, P. Loiseau, G. Piguet, and A. Sabene, "Oversizing array-to-inverter (dc-ac) ratio: What are the criteria and how to define the optimum?" in *Proc. Eur. Photovolt. Sol. Energy Conf. Exhib.*, pp. 2813–2821, Sep. 2014.

[17] R. S. Faranda, H. Hafezi, S. Leva, M. Mussetta, and E. Ogliari, "The optimum PV plant for a given solar dc/ac converter," *Energies*, vol. 8, no. 6, pp. 4853–4870, May 2015.

[18] L. M. Moore and H. N. Post, "Five years of operating experience at a large, utility-scale photovoltaic generating plant," *Progress Photovoltaics: Res. Appl.*, vol. 16, no. 3, pp. 249–259, 2008.

[19] A. Golnas, "PV system reliability: An operator's perspective," *IEEE J. of Photovolt.*, vol. 3, no. 1, pp. 416–421, Jan. 2013.

[20] F. Baumgartner, O. Maier, D. Schar, D. Sanchez, and P. Toggweiler, "Survey of operation and maintenance costs of PV plants in Switzerland," in *Proc. Eur. Photovolt. Sol. Energy Conf. Exhib.*, pp. 1583–1586, Sep. 2015.

[21] P. Hacke, S. Lokanath, P. Williams, A. Vasan, P. Sochor, G. TamizhMani, H. Shinohara, and S. Kurtz, "A status review of photovoltaic power conversion equipment reliability, safety, and quality assurance protocols," *Renewable and Sustainable Energy Reviews*, vol. 82, pp. 1097 – 1112, 2018.

[22] T. J. Formica, H. A. Khan, and M. G. Pecht, "The effect of inverter failures on the return on investment of solar photovoltaic systems," *IEEE Access*, vol. 5, pp. 21 336–21 343, 2017.

[23] A. Sangwongwanich, Y. Yang, D. Sera, and F. Blaabjerg, "Impacts of PV array sizing on PV inverter lifetime and reliability," in *Proc. of ECCE*, pp. 3830–3837, Oct. 2017.

[24] S.B. Kjaer, J.K. Pedersen, and F. Blaabjerg, "A review of single-phase grid-connected inverters for photovoltaic modules," *IEEE Trans. Ind. Appl.*, vol. 41, no. 5, pp. 1292–1306, Sep. 2005.

[25] Y. Yang and F. Blaabjerg, "Overview of single-phase grid-connected photovoltaic systems," *Electric Power Components and Sys.*, vol. 43, no. 12, pp. 1352–1363, 2015.

[26] F. Blaabjerg, R. Teodorescu, M. Liserre, and A.V. Timbus, "Overview of control and grid synchronization for distributed power generation systems," *IEEE Trans. Ind. Electron.*, vol. 53, no. 5, pp. 1398–1409, Oct. 2006.

[27] A. Sangwongwanich, Y. Yang, and F. Blaabjerg, "High-performance constant power generation in grid-connected PV systems," *IEEE Trans. Power Electron.*, vol. 31, no. 3, pp. 1822–1825, Mar. 2016.

[28] M. Musallam, C. Yin, C. Bailey, and M. Johnson, "Mission profile-based reliability design and real-time life consumption estimation in power electronics," *IEEE Trans. Power Electron.*, vol. 30, no. 5, pp. 2601–2613, May 2015.

[29] Y. Yang, H. Wang, F. Blaabjerg, and K. Ma, "Mission profile based multi-disciplinary analysis of power modules in single-phase transformerless photovoltaic inverters," in *Proc. of EPE*, pp. 1–10, Sep. 2013.

[30] Y. Yang, K. Ma, H. Wang, and F. Blaabjerg, "Mission profile translation to capacitor stresses in grid-connected photovoltaic systems," in *Proc. of ECCE*, pp. 5479–5486, Sep. 2014.

[31] C. Felgemacher, S. Araujo, C. Noeding, P. Zacharias, A. Ehrlich, and M. Schidleja, "Evaluation of cycling stress imposed on IGBT modules in PV central inverters in sunbelt regions," in *Proc. of CIPS*, pp. 1–6, Mar. 2016.

[32] V. Smet, F. Forest, J. J. Huselstein, F. Richardeau, Z. Khatir, S. Lefebvre, and M. Berkani, "Ageing and failure modes of IGBT modules in high-temperature power cycling," *IEEE Trans. Ind. Electron.*, vol. 58, no. 10, pp. 4931–4941, Oct. 2011.

[33] H. Wang, M. Liserre, and F. Blaabjerg, "Toward reliable power electronics: Challenges, design tools, and opportunities," *IEEE Ind. Electron. Mag.*, vol. 7, no. 2, pp. 17–26, Jun. 2013.

[34] H. Huang and P. A. Mawby, "A lifetime estimation technique for voltage source inverters," *IEEE Trans. Power Electron.*, vol. 28, no. 8, pp. 4113–4119, Aug. 2013.

[35] Y. Yang, A. Sangwongwanich, and F. Blaabjerg, "Design for reliability of power electronics for grid-connected photovoltaic systems," *CPSS Trans. Power Electron. Appl.*, vol. 1, no. 1, pp. 92–103, 2016.

[36] H. Wang and F. Blaabjerg, "Reliability of capacitors for dc-link applications in power electronic converters - an overview," *IEEE Trans. Ind. App.*, vol. 50, no. 5, pp. 3569–3578, Sep. 2014.

[37] H. Wang, Y. Yang, and F. Blaabjerg, "Reliability-oriented design and analysis of input capacitors in single-phase transformer-less photovoltaic inverters," in *Proc. of APEC*, pp. 2929–2933, Mar. 2013.

[38] D. Sera, R. Teodorescu, and P. Rodriguez, "PV panel model based on datasheet values," in *Proc. of ISIE*, pp. 2392–2396, Jun. 2007.

[39] Enphase Energy, "Reliability study of electrolytic capacitors in a microinverter," Sep. 2008.

[40] U. Scheuermann, R. Schmidt, and P. Newman, "Power cycling testing with different load pulse durations," in *Proc. of PEMD 2014*, pp. 1–6, Apr. 2014.

[41] *Application guide, Aluminum Electrolytic Capacitors*, Cornell Dubilier, Liberty, SC, USA. [Online]. Available: http://www.cde.com/catalogs/AEappGUIDE.pdf

[42] *Type 381LX / 383LX 105 C High Ripple, Snap-In Aluminum*, Cornell Dubilier, Liberty, SC, USA. [Online]. Available: http://http://www.cde.com/resources/catalogs/381-383.pdf

[43] *SGW50N60HS*, Infineon Technologies AG, 2009, rev. 2.3.

[44] P. D. Reigosa, H. Wang, Y. Yang, and F. Blaabjerg, "Prediction of bond wire fatigue of IGBTs in a PV inverter under a long-term operation," *IEEE Trans. Power Electron.*, vol. 31, no. 10, pp. 7171–7182, Oct. 2016.

[45] K. Ma, H. Wang, and F. Blaabjerg, "New approaches to reliability assessment: Using physics-of-failure for prediction and design in power electronics systems," *IEEE Power Electron. Mag.*, vol. 3, no. 4, pp. 28–41, Dec. 2016.

[46] A. Sangwongwanich, Y. Yang, D. Sera, and F. Blaabjerg, "Lifetime evaluation of grid-connected PV inverters considering panel degradation rates and installation sites," *IEEE Trans. Power Electron.*, vol. 33, no. 2, pp. 1225–1236, 2018.

[47] Y. Shen, H. Wang, and F. Blaabjerg, "Reliability oriented design of a grid-connected photovoltaic microinverter," in *Proc. of IFEEC 2017 - ECCE Asia*, pp. 81–86, Jun. 2017.

[48] D. Zhou, H. Wang, and F. Blaabjerg, "Mission profile based system-level reliability analysis of dc/dc converters for a backup power application," vol. PP, no. 99, pp. 1–1, 2017.

[49] H. S.-H. Chung, H. Wang, F. Blaabjerg, and M. Pecht, *Reliability of Power Electronic Converter Systems*. IET, 2015.

[50] Y. Song and B. Wang, "Survey on reliability of power electronic systems," *IEEE Trans. Power Electron.*, vol. 28, no. 1, pp. 591–604, Jan. 2013.

Ariya Sangwongwanich (S'15) received the B.Eng. degree in electrical engineering from Chulalongkorn University, Thailand, in 2013, and the M.Sc. in energy engineering from Aalborg University, Denmark, in 2015, where he is currently working towards his Ph.D. degree.

He was a Visiting Researcher with RWTH Aachen University, Aachen, Germany, from September to December 2017. His research interests include control of grid-connected converter, PV systems, and reliability of power electronic converter systems.

Yongheng Yang (S'12-M'15-SM'17) received the B.Eng. degree in electrical engineering and automation from Northwestern Polytechnical University, Shaanxi, China, in 2009 and the Ph.D. degree in electrical engineering from Aalborg University, Aalborg, Denmark, in 2014.

He was a postgraduate student at Southeast University, China, from 2009 to 2011. In 2013, he was a Visiting Scholar at Texas A&M University, USA. Dr. Yang has been with the Department of Energy Technology, Aalborg University since 2014, first as a Postdoc researcher, then an Assistant Professor, and now an Associate Professor. He has been focusing on grid integration of renewable energies, power electronic converter design, analysis and control, and reliability in power electronics.

Dr. Yang served as a Guest Associate Editor of IEEE JOURNAL OF EMERGING AND SELECTED TOPICS IN POWER ELECTRONICS and a Guest Editor of *Applied Sciences*. He is an Associate Editor of CPSS TRANSACTIONS ON POWER ELECTRONICS AND APPLICATIONS.

Dezso Sera (S'05-M'08-SM'15) received his B.Sc. and M.Sc. degrees in Electrical Engineering from the Technical University of Cluj, Romania in 2001 and 2002, respectively; MSc in Power Electronics and PhD on PV systems from Aalborg University, Denmark, Department of Energy Technology, where he currently works as Associate Professor.

Since 2009 he has been programme leader of the Photovoltaic Systems Research Programme (www.pv-systems.et.aau.dk) at the same dept. His research interests include modelling, characterisation, diagnostics and maximum power point tracking (MPPT) of PV arrays, as well as power electronics and grid integration for PV systems.

Frede Blaabjerg (S'86-M'88-SM'97-F'03) was with ABB-Scandia, Randers, Denmark, from 1987 to 1988. From 1988 to 1992, he was a Ph.D. Student with Aalborg University, Aalborg, Denmark. He became an Assistant Professor in 1992, Associate Professor in 1996, and Full Professor of power electronics and drives in 1998. His current research interests include power electronics and its applications such as in wind turbines, PV systems, reliability, harmonics and adjustable speed drives.

He has received 18 IEEE Prize Paper Awards, the IEEE PELS Distinguished Service Award in 2009, the EPE-PEMC Council Award in 2010, the IEEE William E. Newell Power Electronics Award 2014 and the Villum Kann Rasmussen Research Award 2014. He was an Editor-in-Chief of the IEEE TRANSACTIONS ON POWER ELECTRONICS from 2006 to 2012. He was nominated in 2014, 2015, 2016 and 2017 by Thomson Reuters to be between the most 250 cited researchers in Engineering in the world.

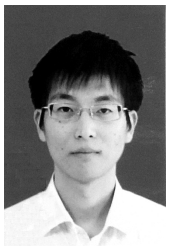

Dao Zhou (S'12-M'15) received the B.S. in electrical engineering from Beijing Jiaotong University, Beijing, China, in 2007, the M. S. in power electronics from Zhejiang University, Hangzhou, China, in 2010, and the Ph.D from Aalborg University, Aalborg, Denmark, in 2014. He is currently a Postdoctoral Researcher in Aalborg University. His research interests include power electronics and reliability in renewable energy application.

Dr. Zhou received the Renewable and Sustainable Energy Conversion Systems of the IEEE INDUSTRY APPLICATIONS SOCIETY First Prize Paper Award in 2015, and Best Session Paper at Annual Conference of the IEEE Industrial Electronics Society (IECON) in Austria in 2013. He serves as a Session Chair for various technical conferences.